

RADIO LOUD AGNs ARE MERGERS

MARCO CHIABERGE^{1,2,3}, ROBERTO GILLI⁴, JENNIFER M. LOTZ¹, AND COLIN NORMAN^{1,5}¹Space Telescope Science Institute, 3700 San Martin Drive, Baltimore, MD 21218, USA²INAF—IRA, Via P. Gobetti 101, Bologna, I-40129, Italy³Center for Astrophysical Sciences, Johns Hopkins University, 3400 N. Charles Street, Baltimore, MD 21218, USA⁴INAF Osservatorio Astronomico di Bologna, via Ranzani 1, I-40127 Bologna, Italy⁵Department of Physics and Astronomy, Johns Hopkins University, Baltimore, MD 21218, USA

Received 2014 December 28; accepted 2015 May 4; published 2015 June 12

ABSTRACT

We measure the merger fraction of Type 2 radio-loud and radio-quiet active galactic nuclei (AGNs) at $z > 1$ using new samples. The objects have *Hubble Space Telescope* (*HST*) images taken with Wide Field Camera 3 (WFC3) in the IR channel. These samples are compared to the 3CR sample of radio galaxies at $z > 1$ and to a sample of non-active galaxies. We also consider lower redshift radio galaxies with *HST* observations and previous generation instruments (NICMOS and WFPC2). The full sample spans an unprecedented range in both redshift and AGN luminosity. We perform statistical tests to determine whether the different samples are differently associated with mergers. We find that all ($92\%_{-14\%}^{+8\%}$) radio-loud galaxies at $z > 1$ are associated with recent or ongoing merger events. Among the radio-loud population there is no evidence for any dependence of the merger fraction on either redshift or AGN power. For the matched radio-quiet samples, only $38\%_{-15}^{+16}$ are merging systems. The merger fraction for the sample of non-active galaxies at $z > 1$ is indistinguishable from radio-quiet objects. This is strong evidence that mergers are the triggering mechanism for the radio-loud AGN phenomenon and the launching of relativistic jets from supermassive black holes (SMBHs). We speculate that major black hole (BH)–BH mergers play a major role in spinning up the central SMBHs in these objects.

Key words: galaxies: active – galaxies: interactions – galaxies: jets – galaxies: nuclei – X-rays: galaxies

1. INTRODUCTION

One of the most important issues in modern astrophysics is understanding the co-evolution of galaxies and their central supermassive black holes (SMBHs; Heckman & Best 2014; Alexander & Hickox 2012, for recent reviews on the subject). Both numerical simulations and theoretical arguments show that black hole (BH) growth occurs during short-lived periods ($\sim 10^7$ – 10^8 years) of intensive accretion that are also associated with powerful quasar activity (Soltan 1982; Rees 1984; Di Matteo et al. 2005; Hopkins et al. 2008b; Somerville et al. 2008). These are also expected to correspond to periods in which galaxies grow hierarchically. Since the matter that ultimately accretes onto the central BH needs to lose almost all ($\sim 99.9\%$) of its angular momentum, studies of mergers, tidal interactions, stellar bars, and disk instabilities are central for understanding the details of such a process. Numerical simulations and analytic calculations have shown that major (gas-rich) mergers are capable of efficiently driving gas inflows toward the central region of the galaxy ($\lesssim 1$ kpc) through tidal forces (e.g., Hernquist 1989; Di Matteo et al. 2005; Li et al. 2007; Hopkins & Quataert 2011), and ultimately drive the gas to the central ~ 1 pc, forming an accretion disk around the central SMBH (Hopkins & Quataert 2010). This is also thought to be a likely scenario for the formation of galaxy spheroids (e.g., Hopkins et al. 2008a). However, disk instabilities and minor mergers may also be able to provide material for BH accretion (e.g., Hernquist & Mihos 1995; Menci et al. 2014).

It is extremely important to study the connection between galaxy and BH growth from a purely observational point of view. One of the central questions is whether mergers or other mechanisms may constitute the main triggering mechanisms for active galactic nuclei (AGNs). A number of recent papers

investigated this issue using data from different surveys of galaxies and AGNs. Results are often contradictory. Although it is known that not all of them are AGNs, powerful Ultra-Luminous Infrared Galaxies (ULIRG) are ubiquitously associated with major mergers (Sanders & Mirabel 1996; Veilleux et al. 2002). According to some models (e.g., Hopkins et al. 2008a, 2008b) these objects are believed to represent a fundamental stage in the process of the formation of elliptical galaxies. Kartaltepe et al. (2012) showed that for a sample of $z \sim 2$ ULIRGs in the GOODS-South field (Giavalisco et al. 2004), the fraction of mergers is up to $\sim 70\%$. For lower luminosities objects (LIRGs) in the same redshift range the merger fraction found by the same authors is significantly smaller ($\sim 30\%$).

While the merger–ULIRG connection seems to be well established, whether this is a viable scenario for all AGNs is still an unanswered question. Bahcall et al. (1997) observed a sample of 20 relatively nearby QSOs with the *Hubble Space Telescope* (*HST*) and found that the majority of them reside in merging galaxies. Grogan et al. (2003) studied the optical counterparts of the X-ray selected AGNs from the 1 Msec *Chandra* Deep Field South (Giacconi et al. 2002). Based on both the asymmetry index and the frequency of close companions, these authors concluded that mergers and interactions are not good indicators of AGN activity. Interestingly, using *HST* images taken with the Wide Field Camera 3 (WFC3) Schawinski et al. (2012) showed that only a small fraction of heavily obscured QSO hosts are associated with mergers. Treister et al. (2012) put together a relatively large sample of literature data and found clues for a luminosity dependence of the merger fraction in both ULIRGs and AGNs. On the other hand, Villforth et al. (2014) showed that their sample of QSOs observed with *HST* did not show any evidence for a dependence of the merger fraction on luminosity.

Recently, based on a sample of SDSS galaxies, Sabater et al. (2015) found that the effect of interactions is minimal in triggering AGN activity.

A major issue is related to the so-called radio-loud/radio-quiet dichotomy of active nuclei. It has been long argued that in order to produce powerful relativistic jets, radio-loud AGNs must possess an extra source of energy with respect to radio-quiet AGNs. The most popular scenarios among those proposed so far assume that the energy may be extracted from the innermost region of a magnetized accretion disk around a rapidly spinning BH (Blandford & Znajek 1977). In the Blandford–Znajek framework, the radio-quiet/radio-loud dichotomy can be explained in terms of a corresponding low/high BH spin separation (Blandford et al. 1990, p. 97). Alternative models predict that jets are directly powered by the accretion disk (Blandford & Payne 1982; Pudritz & Norman 1986; Xu et al. 1999). Both theoretical arguments and observational evidence support the Blandford–Znajek scenario (see, e.g., Ghisellini et al. 2014). Recent numerical simulations also seem to confirm such a mechanism as a viable physical explanation for efficient jet production (e.g., McKinney & Gammie 2004; Hawley & Krolik 2006; Tchekhovskoy et al. 2011; Sądowski et al. 2015). Wilson & Colbert (1995) originally proposed that radio-loud AGNs are associated with rapidly spinning BHs that are ultimately spun-up by major BH–BH mergers. It is clear that a straightforward prediction of such a scenario is that radio galaxies and radio-loud QSOs (RLQSOs) should exhibit signatures of major galaxy mergers.

Radio-loud AGNs are known to be hosted by large elliptical galaxies and are associated with SMBH of at least $\sim 10^8 M_{\odot}$ (e.g., Laor 2000; Dunlop et al. 2003; Best et al. 2005; Chiaberge & Marconi 2011). Furthermore, these objects are present in more richer environments (clusters and groups of galaxies) than radio-quiet AGNs (Shen et al. 2009; Donoso et al. 2010; Ramos Almeida et al. 2013) and they are often associated with brightest cluster galaxies (Best et al. 2007). At least a fraction of them have been known to be associated with merging system for a long time (e.g., Heckman et al. 1986; Colina & de Juan 1995). Recently, Ramos Almeida et al. (2012) studied samples of relatively low-redshift ($z < 0.7$) sources with deep ground based observations. These authors found that the large majority ($\sim 80\%$) of radio-loud objects show disturbed morphologies. The same group also studied a small sample of radio-quiet Type 2 quasars (Bessiere et al. 2012) and found that the merger fraction sample is as high as 75%.

However, an accurate census of the merger fraction in carefully selected samples of AGNs over a large range of redshift, luminosity, and radio-loudness is still needed to provide a final answer to the above questions. This should also be based on a homogeneous set of deep, high spatial resolution observations and supported by firm statistical evidence for any difference in the observed merger fractions among the different samples. The aim of this paper is to make a significant step toward such a goal.

With the aim of determining the importance of mergers in triggering different types of AGN activity, we select samples of both radio-loud and radio-quiet Type 2 AGNs. In this paper we focus on Type 2 objects only, because the bright nuclear component that dominates the emission on Type 1 AGNs (QSOs) hampers a detailed morphological study of both the host galaxies and the close environment of those objects. This

constitutes a serious concern, particularly at moderate to high redshifts, even using *HST* images. In this work we focus on objects with $1 < z < 2.5$. This is a range of redshift where the peak of the AGN activity is believed to occur, and where mergers play a dramatic role in the late evolution of massive galaxies (e.g., Hopkins et al. 2008b). The availability of *HST* data for a substantial number of objects in each sample is key to this work. In particular, we focus on samples observed with WFC3 and the IR channel. The extremely high sensitivity, low background level and the range of wavelengths covered by such an instrument is particularly suitable to our goals. In fact, the rest frame wavelength corresponding to the most widely used WFC3-IR filters (i.e., F140W and F160W) is still well within the optical range for objects in the redshift range of our interest. Even in relatively short exposures (i.e., a few hundreds seconds, or less than 1 *HST* orbit) the effects of merger events on the structure of galaxies are clearly revealed in WFC3-IR images. This is possible thanks to the high sensitivity in the near-IR coupled with the large field of view of WFC3, compared to previous generation instruments such as WFPC2, NICMOS and ACS.

In Section 2 we describe the samples and the observations analyzed in this work, while in Section 3 we discuss our method to classify mergers based on visual inspection of the *HST* images. In Section 4 we describe the statistical analysis of the results. In Section 5 we discuss our findings and we outline our framework for their interpretation in Section 6. Finally, in Section 7 we summarize our results and we draw conclusions.

Throughout the paper we assume $\Omega_M = 0.3$, $\Omega_{\lambda} = 0.7$, and $H_0 = 70 \text{ Km s}^{-1} \text{ Mpc}^{-1}$. For the magnitude system, we use AB magnitudes.

2. THE SAMPLE

One fundamental goal of this work is to establish whether there is a significant difference in the role played by mergers among different classes of AGNs and for different bins of redshift and bolometric power. To this aim, we use well defined samples of classical radio galaxies spanning 5 dex in radio power. We also select new samples of both radio-quiet and radio-loud AGNs, as well as non-active galaxies at $z > 1$. In doing so, we use particular care in separating the radio-quiet and radio-loud populations, as explained below.

In the following we describe the properties of each of the samples used as part of this work, together with the selection criteria used to derive new samples.

2.1. Radio Loud AGNs: $z > 1$ 3CR Radio Galaxies

The first sample we consider is composed by the radio galaxies with $z > 1$ from the 3CR catalog (Spinrad et al. 1985). These are all powerful radio galaxies belonging to the Fanaroff–Riley class II (FR II; Fanaroff & Riley 1974), i.e., those in which the brightest components of the radio structure lie at the edges of the radio source, in contrast to the FR Is, in which the peak of the radio emission is located at the core.

The 3CR is a flux limited sample selected at low radio frequencies ($S_{178} > 9 \text{ Jy}$ at 178 MHz). Since the radio emission at such frequencies is dominated by the radio lobes, the selection is independent of the AGN orientation. The original catalog includes both Type 1 (QSOs) and Type 2 objects (radio galaxies) and it is one of the best studied samples of radio-loud AGNs, being perfectly suitable to test AGN unification

scenarios. The high redshift objects included in the 3CR are all firmly established radio-loud AGNs with powerful relativistic jets emanating from the central SMBH. Even at the lowest luminosities, the active nucleus is strongly radio-loud (see e.g., Chiaberge et al. 2005; Sikora et al. 2007), assuming the canonical threshold $R = F_{5\text{ GHz}}/F_B > 10$ (Kellermann et al. 1989), where $F_{5\text{ GHz}}$ and F_B are the fluxes in the radio band at 5 GHz and in the optical B band, respectively. The $z > 1$ sub-sample of the 3CR catalog includes 58 objects. The highest redshift object is the radio galaxy 3C257 at $z = 2.47$.

The radio power of these AGNs is $L_{151} \sim 10^{35} \text{ erg s}^{-1} \text{ Hz}^{-1}$ or slightly higher, which corresponds to a bolometric luminosity $L_{\text{bol}} \sim 10^{45-46} \text{ erg s}^{-1}$ assuming standard bolometric corrections. This result is also supported by the estimates of the X-ray luminosity for some of these objects, which is typically in the range $L_{2-10} \sim 10^{44-45} \text{ erg s}^{-1}$. Salvati et al. (2008) observed a sample of the most luminous and most distant radio galaxies and QSOs from the 3CR catalog with *XMM*. They found that the intrinsic X-ray luminosity is in the range $6 \times 10^{44} < L_{2-10\text{ keV}} < 2 \times 10^{46} \text{ erg s}^{-1}$, the Type 1 QSOs being a factor of ~ 6 or higher brighter than the (Type 2) radio galaxies. These authors interpreted such a discrepancy as a result of the presence of a beamed component in the Type 1 QSOs. Wilkes et al. (2013) found similar results based on *Chandra* data. E. Torresi et al. (2015, private communication) analyzed both *Chandra* and *XMM* archival data for the 3CR radio galaxies observed with *HST*, and found intrinsic X-ray luminosities as low as $L_{2-10\text{ keV}} \sim 2 \times 10^{44} \text{ erg s}^{-1}$. However, the absorbing column density is poorly constrained, and it is possible that at least some of the Type 2 radio galaxies are in fact Compton-thick. In that case, the derived X-ray luminosity sets a lower limit to the intrinsic AGN luminosity in that band.

Twelve 3CR radio galaxies were observed with WFC3-IR and the F140W filter (in addition to WFC3-UVIS and F606W, not used in this work) as part of program SNAP13023 (PI M. Chiaberge, B. Hilbert et al. 2015, in preparation). The wide-band filter used for the *HST* observations (F140W) includes emission lines at the redshift considered here (mainly $\text{H}\alpha$, $\text{H}\beta$, and/or $[\text{O III}]5007$, depending on the redshift of the source). However, the only object that is significantly contaminated by line emission is 3C 230 (see Steinbring 2011). The *HST* image of this specific object only shows the narrow-line region and thus we cannot observe the stellar component of the host. Therefore we exclude this source from our sample.⁶ *HST* snapshot surveys of complete samples are well suitable for statistical studies, since the observations are scheduled by randomly picking objects from the original target list to fill gaps in the *HST* schedule. The observed sample spans the entire range of redshift of the original list, i.e., from $z = 1.0$ to 2.47. The comparison samples described in the following are tailored to match the properties of these 3CR galaxies, in either bolometric power or redshift range (or both).

⁶ A quick inspection of the images from the *HST*-SNAP13023 program shows that 3C 230 is the only object that presents an identical structure in both of the observed bands which is easily recognizable as due to emission line filaments. All other objects show, in the filter used in this work, a much smoother morphology that is not typical of emission line regions. The bandwidth of F140W is extremely wide ($\sim 0.4 \mu\text{m}$), therefore the expected emission line contamination is small. In fact, for all radio galaxies except for 3C 230, we estimate that, based on the observed emission line flux from ground based spectra, the total emission line contamination does not exceed 20% of the total observed flux (B. Hilbert et al. 2015, in preparation). Similar considerations hold for the other samples used in this work.

In Table 1 we report the data for the 11 sources belonging to this sample. The $24 \mu\text{m}$ luminosities taken from Podigachoski et al. (2015) are used in the following to check that the relevant comparison sample is correctly matched to the Hz3C.

In Figure 1 we show the location of the 3CR sample in the radio power versus redshift plane, with respect to other samples used throughout the paper. Note that, at any redshift, 3CR objects are always the most powerful radio sources.

2.2. Radio Loud AGNs: Low-luminosity Radio Galaxies at $1 < z < 2.5$

The sample of high redshift low-luminosity radio galaxies (HzLLRGs) is derived from the Extended *Chandra* Deep Field South (ECDFS Lehmer et al. 2005). We use the Bonzini et al. (2012) catalog and AGN type classification to derive this sample. The criteria are as follows.

- (i) The spectroscopic, if available, or photometric redshift of the source must be in the range $1 < z < 2.5$. The redshift range is chosen to roughly match the range spanned by the 3CR sample described above.
- (ii) The total radio power at 1.4 GHz must be greater than $P_{1.4\text{ GHz}} > 10^{30} \text{ erg s}^{-1} \text{ Hz}^{-1}$ and below the fiducial FRI/FRII separation $P_{1.4\text{ GHz}} < 4 \times 10^{32} \text{ erg s}^{-1} \text{ Hz}^{-1}$ (Fanaroff & Riley 1974).
- (iii) The source must be classified as a radio-loud AGN by Bonzini et al. (2013), i.e., it must show radio emission in excess of that produced by starbursts. This is measured by using the $q_{24\text{ obs}}$ parameter, defined as $q_{24\text{ obs}} = \log(S_{24\text{ obs}}/S_r)$, where $S_{24\text{ obs}}$ is the observed flux density at $24 \mu\text{m}$ and S_r is the observed flux density at 1.4 GHz. Bonzini et al. (2013) define an object as radio-loud if $q_{24\text{ obs}}$ is 2σ off of the starburst locus, defined using the M82 template (see their Figure 2).
- (iv) We also impose the additional constraint that its X-ray luminosity must not exceed $L_{2-10\text{ keV}} = 10^{44} \text{ erg s}^{-1}$. This is to ensure that the objects are consistent with typical low power radio galaxies at both low and high redshifts (e.g., Balmaverde et al. 2006; Tundo et al. 2012). The upper limit to the X-ray luminosity is also consistent with the results of Terashima & Wilson (2003). These authors showed that the radio-loud–radio-quiet dichotomy can be redefined using the X-ray emission instead of the flux in the optical band. This is particularly useful for Type 2 AGNs such as the ones considered in this work, since the optical emission from the accretion disk is heavily obscured in these object. According to such a scheme, powerful radio-loud AGNs are present for $R_X \gtrsim -3.5$, where R_X is defined as the logarithm of the ratio between the radio luminosity (νL_ν) at 1.4 GHz and the X-ray luminosity L_{2-10} . At low radio powers, it is easy to confuse a powerful radio-quiet AGN that shows some radio emission with a radio-loud object that is intrinsically weak at all wavelengths. Note that our selection criteria for the radio and X-ray luminosities correspond to $R_X > -2.3$, which is a rather conservative value. We prefer to follow a conservative approach because for low-luminosity AGNs the transition between radio-quiet and radio-loud most likely occurs at higher values than for high power objects, similarly to the classical radio-loudness parameter R derived using the radio-to-optical

Table 1
High- z 3CR Radio Galaxies

| Name | R.A. (2000.0) hh:mm:ss.ss | Decl. (2000.0) dd:mm:ss.ss | Redshift z | $\log R_{1.4\text{GHz}}$ $\log[\text{erg s}^{-1} \text{Hz}^{-1}]$ | $L_{24\mu\text{m}}$ $\log[\text{erg s}^{-1} \text{Hz}^{-1}]$ |
|----------|------------------------------|-------------------------------|-----------------|--|---|
| 3C 210 | 08:58:10.0 | +27:50:52 | 1.169 | 35.13 | 45.65 |
| 3C 255 | 11:19:25.2 | -03:02:52 | 1.355 | 35.29 | <44.54 |
| 3C 257 | 11:23:09.2 | +05:30:19 | 2.474 | 35.94 | 45.94 |
| 3C 297 | 14:17:24.0 | -04:00:48 | 1.406 | 35.33 | 44.84 |
| 3C 300.1 | 14:28:31.3 | -01:24:08 | 1.159 | 35.37 | ... |
| 3C 305.1 | 14:47:09.5 | +76:56:22 | 1.132 | 35.10 | 45.36 |
| 3C 322 | 15:35:01.2 | +55:36:53 | 1.168 | 35.20 | 44.90 |
| 3C 324 | 15:49:48.9 | +21:25:38 | 1.206 | 35.34 | 45.48 |
| 3C 326.1 | 15:56:10.1 | +20:04:20 | 1.825 | 35.75 | 45.64 |
| 3C 356 | 17:24:19.0 | +50:57:40 | 1.079 | 34.96 ^a | 45.52 |
| 3C 454.1 | 22:50:32.9 | +71:29:19 | 1.841 | 35.60 | 45.67 |

Note. $P_{1.4}$ from Condon et al. (1998) except for item ^a from Laing & Peacock (1980). The $24\mu\text{m}$ luminosities are derived from the fluxes published in Podigachoski et al. (2015).

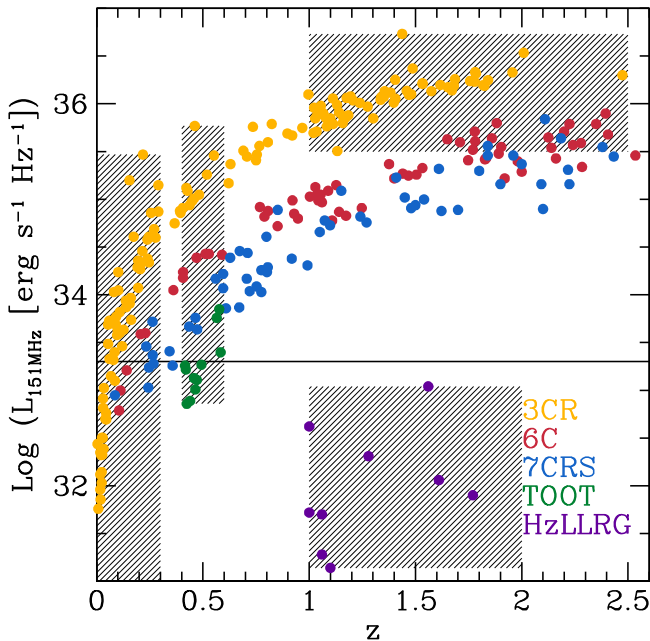


Figure 1. Radio loud samples considered in this paper. The horizontal line represents the canonical separation between low and high power radio galaxies (i.e., FR I and FR II, respectively). The color code identifies the different catalogs, and the shaded area show the regions of the radio luminosity vs. redshift plane where *HST* observations are suitable for this paper (see the text). Here, the $z < 0.3$ range is covered by the 3CR sources (yellow), and the four groups that are part of the Willott sample (6C, 7C, and TOOT are in red, blue, and green, respectively) plus the 3CR with $z \sim 0.5$ cover the range around $z = 0.5$. Both the low- z 3CR and the Willott sample are described in Section 4.1. The $z > 1$ range is covered again by the 3CR at high luminosity, and by the ECDFS HzLLRGs (purple) at the lowest luminosities. See Section 2 for more details.

luminosity ratio (Terashima & Wilson 2003; Chiaberge et al. 2005; Sikora et al. 2007).

- (v) The source must be observed with *HST* WFC3-IR. Most of the images are taken from the CANDELS survey (Grogin et al. 2011; Koekemoer et al. 2011), or from surrounding fields observed as part of program GO-12866 (see Table 2). The ECDF sample includes six HzLLRGs.

We also use the same criteria to select HzLLRG in the CANDELS UDS field in the Subaru/*XMM Newton* Deep field survey (Ueda et al. 2008). The radio data are from Simpson

et al. (2012), the $24\mu\text{m}$ *Spitzer* IR data are taken from the *Spitzer* Public Legacy Survey of the UKIDSS Ultra Deep Survey (SpUDS, P.I. J.S. Dunlop) using the IRSA database. Only two galaxies that satisfy our selection criteria lie in the region covered by the *HST* WFC3 observations.

The properties of the eight galaxies included in the HzLLRG sample are reported in Table 2. In Figure 1 we show the radio power versus redshift distribution of these AGNs, compared with the other radio-loud samples. Note that the two radio-loud samples at $z > 1$ used in this paper (i.e., the 3CR and the HzLLRGs) are separated by about 4 dex in radio power, on average.

2.3. Radio Quiet AGNs: Low-power Type 2 AGNs at $1 < z < 2.5$

The sample of low-power Type 2 AGNs (LPTy2AGN) is selected from the 4Msec CDFS catalog and source classification (Xue et al. 2011). We include objects that are classified as AGNs, that do not show strong broad emission lines in the optical spectrum, and whose redshift is $1.0 < z < 2.5$. We also use the additional constraint that the intrinsic (de-absorbed) X-ray luminosity (integrated between 2 and 10 keV, in the rest frame of the source) must be $L_{2-10\text{keV}} < 2 \times 10^{42} \text{ erg s}^{-1}$, in order to be consistent with the properties of the corresponding radio-loud sample described in Section 2.2. The $L_{2-10\text{keV}}$ luminosity is derived from the 0.5–8 keV luminosity listed in the catalog, converted to the 2–10 keV band using a photon index $\Gamma = 1.8$. Furthermore, for the objects that are detected in the radio, we require that the X-ray radio-loudness parameter R_X defined in Section 2.2 is < -3.5 . The sample includes 26 objects. These are very low-power AGNs that are similar to Seyfert 2 galaxies in the local Universe. The properties of these AGNs are reported in Tables 3. The *HST*/WFC3-IR images for this sample are taken from the CANDELS survey (Grogin et al. 2011; Koekemoer et al. 2011).

2.4. Radio Quiet AGNs: High-power Type 2 AGNs at $1 < z < 2.5$

As for the low-power AGNs described above, the sample of high-power Type 2 AGNs (HPTy2AGN) is drawn from the CDFS. When selecting this sample we want to match as close as possible both the redshift range and the bolometric luminosity of the powerful 3CR radio galaxy sample.

Table 2
High- z Low Luminosity Radio Galaxies

| ID | R.A. (2000.0) hh:mm:ss.ss | Decl. (2000.0) dd:mm:ss.ss | Redshift z | <i>HST</i> Survey or Prog. ID | $\log R_{1.4\text{GHz}}$ $\log[\text{erg s}^{-1} \text{Hz}^{-1}]$ | $\log L_{2-10}$ $\log[\text{erg s}^{-1}]$ | q_{24} |
|-------|------------------------------|-------------------------------|-------------------|-------------------------------|--|--|----------|
| ECDFS | | | | | | | |
| 65 | 03:31:23.30 | -27:49:05.80 | 1.10 ^a | 12866 | 31.85 | <42.56 | -1.54 |
| 127 | 03:31:34.13 | -27:55:44.40 | 1.06 | 12866 | 30.51 | <42.69 | -0.09 |
| 215 | 03:31:50.74 | -27:53:52.15 | 1.77 | 12866 | 31.13 | <42.69 | -0.46 |
| 338 | 03:32:10.79 | -27:46:27.80 | 1.61 ^b | CANDELS | 31.29 | 42.43 | -0.98 |
| 410 | 03:32:19.30 | -27:52:19.38 | 1.10 ^b | CANDELS | 30.37 | <42.27 | -0.23 |
| 412 | 03:32:19.51 | -27:52:17.69 | 1.06 | CANDELS | 30.93 | <42.24 | -0.51 |
| UDS | | | | | | | |
| 48 | 02 18 18.38 | -05 15 45.2 | 1.56 | CANDELS | 32.27 | <43.93 | 0.09 |
| 124 | 02 17 04.77 | -05 15 18.1 | 1.28 ^b | CANDELS | 31.54 | <43.73 | -0.50 |

Note. For the ECDFS sources the ID corresponds to the source ID in the Bonzini et al. (2012) catalog. For the UDS galaxies, the ID is the Simpson et al. (2012) source number. Redshifts are photometric redshifts from Bonzini et al. (2012), except where stated otherwise. The UDS sources are undetected in the X-rays.

^a Photometric redshift from Cardamone et al. (2010).

^b Spectroscopic redshift.

Table 3
Radio Quiet Low Power Ty2 AGNs at $1 < z < 2.5$

| ID | R.A. hh:mm:ss.s | Decl. dd:mm:ss.s | Redshift z | $\log L_{2-10}$ $\log[\text{erg s}^{-1}]$ |
|------------------------------|--------------------|---------------------|-----------------|--|
| Low Power Type 2 AGNs (CDFs) | | | | |
| 125 | 03:32:06.77 | -27:49:14.10 | 1.050 | 42.04 |
| 147 | 03:32:09.22 | -27:51:43.50 | 1.352 | 41.99 |
| 216 | 03:32:15.26 | -27:44:38.60 | 1.109 | 41.70 |
| 225 | 03:32:15.91 | -27:48:02.20 | 1.520 | 41.90 |
| 226 | 03:32:16.04 | -27:48:59.90 | 1.413 | 41.91 |
| 247 | 03:32:17.84 | -27:52:10.80 | 1.760 | 42.15 |
| 317 | 03:32:23.16 | -27:45:55.00 | 1.224 | 42.25 |
| 318 | 03:32:23.17 | -27:44:41.60 | 1.571 | 42.09 |
| 321 | 03:32:23.61 | -27:46:01.40 | 1.033 | 41.98 |
| 376 | 03:32:27.04 | -27:53:18.60 | 1.103 | 41.88 |
| 389 | 03:32:28.62 | -27:45:57.20 | 1.626 | 41.97 |
| 394 | 03:32:28.85 | -27:47:56.00 | 1.383 | 41.89 |
| 416 | 03:32:29.94 | -27:52:52.80 | 1.017 | 41.76 |
| 419 | 03:32:30.05 | -27:50:26.80 | 1.005 | 41.48 |
| 428 | 03:32:31.11 | -27:49:40.00 | 1.508 | 41.79 |
| 455 | 03:32:33.06 | -27:48:07.80 | 1.188 | 41.75 |
| 462 | 03:32:33.67 | -27:47:51.20 | 1.388 | 41.84 |
| 463 | 03:32:33.84 | -27:46:00.60 | 1.903 | 42.09 |
| 491 | 03:32:35.80 | -27:47:35.10 | 1.223 | 42.13 |
| 493 | 03:32:35.98 | -27:48:50.70 | 1.309 | 42.19 |
| 504 | 03:32:36.35 | -27:49:33.40 | 1.508 | 41.81 |
| 536 | 03:32:39.07 | -27:53:14.80 | 1.380 | 41.98 |
| 541 | 03:32:39.42 | -27:53:12.70 | 1.381 | 42.00 |
| 545 | 03:32:39.65 | -27:47:09.60 | 1.317 | 41.88 |
| 558 | 03:32:41.01 | -27:51:53.40 | 1.476 | 42.19 |
| 579 | 03:32:43.45 | -27:49:02.20 | 1.603 | 41.97 |

Note. The ID corresponds to the source ID in the Xue et al. (2011) catalog. The redshifts (z_{adopt} in the Xue et al. catalog) are spectroscopic, if available, or photometric. The intrinsic X-ray luminosities (converted to the 2–10 keV band as explained in the text) are also from Xue et al. (2011).

The sample of HPTy2AGN includes objects classified as AGN with redshift $1 < z < 2.5$ and intrinsic X-ray luminosity $L_{2-10\text{keV}} > 10^{44} \text{ erg s}^{-1}$. The lower limit in X-ray power is chosen to match the properties of the 3CR sample described in Section 2.1. Two of the objects (166 and 577) show relatively broad Mg II and C III] emission lines in the optical spectrum (Szokoly et al. 2004). However, the *HST* images clearly show

Table 4
Radio Quiet High Power Ty2 AGNs at $1 < z < 2.5$

| ID | R.A. hh:mm:ss.s | Decl. dd:mm:ss.s | Redshift z | $\log L_{2-10}$ $\log[\text{erg s}^{-1}]$ | $\log L_{24\mu\text{m}}$ $\log[\text{erg s}^{-1}]$ |
|-----|--------------------|---------------------|-----------------|--|---|
| 166 | 03:32:10.93 | -27:44:15.20 | 1.605 | 44.21 | 44.81 |
| 243 | 03:32:17.19 | -27:52:21.00 | 1.097 | 44.05 | 44.39 |
| 257 | 03:32:18.35 | -27:50:55.61 | 1.536 | 44.07 | 44.30 |
| 278 | 03:32:20.07 | -27:44:47.51 | 1.897 | 44.06 | 45.04 |
| 351 | 03:32:25.70 | -27:43:06.00 | 2.291 | 44.31 | 45.46 |
| 518 | 03:32:37.77 | -27:52:12.61 | 1.603 | 44.23 | 45.38 |
| 577 | 03:32:43.24 | -27:49:14.50 | 1.920 | 44.12 | 44.70 |
| 713 | 03:33:05.90 | -27:46:50.70 | 2.202 | 44.02 | ... |
| 720 | 03:33:07.64 | -27:51:27.30 | 1.609 | 44.39 | ... |

Note. The ID corresponds to the source ID in the Xue et al. (2011) catalog. The redshifts (z_{adopt} in the Xue et al. catalog) are spectroscopic, if available, or photometric. The intrinsic X-ray luminosities (converted to the 2–10 keV band as explained in the text) are also from Xue et al. (2011). The $24 \mu\text{m}$ luminosities are from Cardamone et al. (2008).

the host galaxy and there is no evidence for the presence of any strong unresolved nuclear source, as it would be expected for a powerful Type 1 QSO. Therefore, for the purpose of this work, we consider those two objects as Type 2, regardless of the presence of broad lines.

As for the LPTy2AGN, for the objects that are detected in the radio, we require that the X-ray radio-loudness parameter R_X defined in Section 2.2 is < -3.5 . This sample includes 9 AGNs (see Table 4). The *HST*/WFC3-IR images for this sample are taken from the CANDELS survey (Grogin et al. 2011; Koekemoer et al. 2011).

Since the X-ray luminosity might be poorly constrained because of the uncertainty on the amount of nuclear obscuration, we should also make sure that this sample and the Hz3Cs have similar mid-IR luminosities. We performed a K–S test to check whether the distributions of $24 \mu\text{m}$ luminosity of the Hz3C and HPTy2AGN are different.⁷ The resulting p -value is $p = 0.1$, therefore we cannot reject the null

⁷ Note that we did not perform the same test for the LPTy2AGN because those are all undetected at $24 \mu\text{m}$.

hypothesis that the two distributions are drawn from the same population.

2.5. Non-active Galaxies at $1 < z < 2.5$

This sample is derived from the 3D-*HST* survey of the GOODS-SOUTH field (Giavalisco et al. 2004; Brammer et al. 2012; Skelton et al. 2014). We select galaxies with spectroscopic redshift $1 < z < 2.5$ and with magnitude in the F140W filter $19 < m_{F140W} < 22$. The magnitude range is chosen to match the magnitudes of the 3CR radio galaxies from Section 2.1 (B. Hilbert et al. 2015, in preparation). The full sample includes 145 galaxies. We limit the sample to the 50 objects included in the southern half area of the field observed with WFC3-IR and the F140W filter as part of the 3D-*HST* survey. Five of these objects are AGNs, therefore we are left with a sample of 45 galaxies. These are sufficient to provide us a statistically sound sample to be compared with the active galaxy samples described above. We refer to this sample as the *bright* sample of non-active galaxies. Note that we could in principle derive a larger sample by using the full area covered by the 3D-*HST* image of the GOODS-S field. However, this would not significantly improve the statistics for a sample that is already the largest we consider.

In the same area of the sky, we also select a comparable sample of fainter galaxies ($22 < m_{K_s} < 24$) from the same *HST* survey. This sample spans the same magnitude range as the bulk of our radio-quiet AGN population. In the following, we will refer to this sample as the *faint* galaxies sample.

Even if we are selecting objects in the very same redshift range, the near-IR (rest-frame optical) magnitude might not be a good tracer of the stellar mass because of the possible presence of obscuration in some objects. We do not believe that this might significantly affect our results. However, in order to perform a sanity check, we also select a sample of non-active galaxies in the full GOODS-S area of 3D-*HST* matched to the stellar mass estimates of the Hz3C galaxies. At $1 < z < 2.5$ these are typically between 1×10^{11} and $5 \times 10^{11} M_{\odot}$ (Seymour et al. 2007), although a small number of lower mass objects are also present. Although stellar mass measurements based on SED fitting heavily rely on models, it is important to check that our non-active galaxy samples are correctly representing the population of objects we need for comparison. If we restrict our range of masses between the above values, and after excluding those that are AGNs, we obtain 23 objects. About half of them are in common with the *bright* sample. While we do not consider this as our main control sample of non-active galaxies, results for this sample are briefly discussed in Section 4, for the sake of completeness.

The *HST*/WFC3-IR images are taken as part of the 3DHST survey with the F140W filter.

3. MERGER FRACTION

In order to measure the merger fraction we use at least four human classifiers for each sample. For the Hz3C and the Ty2 AGN samples we used six classifiers, to be sure that the authors of the paper were not biased a priori toward any specific result. Each classifier visually inspects all of the targets. While being qualitative in nature, visual classification has been proven to be an effective way of classify mergers, since the eye can pick all of the different signatures of such events. On the other hand, quantitative methods using the Gini coefficient G , the

concentration index C , the asymmetry index A , or the second-order moment of the brightest 20% of the light (M_{20}) only select particular mergers that each of the above indicators are able to identify (Lotz et al. 2011). Therefore, if we use any of those methods we would derive smaller merger fractions.

We classify objects as mergers (or post-mergers) if clear signatures of a mergers are present. These include the presence of double/multiple nuclei, close pairs, tidal tails, bridges, or distorted morphologies clearly indicating a recent or ongoing merger. Close pairs are defined using a projected separation of less than 25 kpc between the center of the galaxies involved, corresponding to 3 arcsec in the redshift range spanned by our $z > 1$ samples.⁸ Such a scale is similar to the typical separations observed in galaxy pairs at low redshifts (e.g., Smith & Heckman 1989; Behroozi et al. 2015).⁹

When possible, mergers are also visually distinguished between *major* and *minor*, assuming the usual separation at a $\sim 4:1$ mass/apparent brightness ratio (e.g., Lotz et al. 2011). If there is no clear evidence for any of the above properties, we classify the object as a *non-merger*. For the AGN samples, a *blind* classification is performed, i.e., classifiers did not know whether each object was radio-loud or radio-quiet, and if it belonged to the high- or low-power class. Classifiers are also asked to classify objects more than once (typically twice).

While substantial agreement exists between the different classifiers for most of the objects, different people may see different features in each image, thus the classification for single sources may differ. This is why we do not report the merger classification for each galaxy in the tables. In order to reduce the effects of large deviations among the different classifiers we calculate 10%-trimmed means for each sample.¹⁰ We report the results for each of the samples at $z > 1$ in Table 5.

Examples of the morphologies observed in the different samples are given in Figures 2, 3, and 4. In order to avoid confusion between our merger classification criteria, we use the figures to give a few specific examples. 3C 297 and 3C356 in Figure 2 are both classified as mergers based on those clear signatures of interaction. 3C 297 also shows a double nucleus. Although not all cases are as straightforward as these, similar considerations can be made for objects in the other samples (see, e.g., the systems shown in the right panes of both Figures 3 and 4). In particular, the objects shown in Figure 3 are most likely examples of dry mergers in which the galaxy isophotes are highly asymmetric (see, e.g., Bell et al. 2006). The central panels of Figure 4 show objects that some of the classifiers classified as mergers, while others did not. Those that classified the objects as mergers noticed some asymmetries

⁸ Between $z = 1$ and $z = 2.5$ the projected scale varies by less than 0.1 arcsec.

⁹ Note that the definitions of “double nucleus” and “close pair” are only formally different. For the purposes of our work, these objects are in fact the same. The different names only identify the appearance of the object in the image, since our classification is based on visual inspection. We classify the object as a double (or multiple) nucleus if the two objects are not clearly separated and they appear to lie within a common envelope. If the galaxies are well separated, but their nuclei are less than ~ 25 kpc apart, then we call it a close pair. However, it is important to note that all of these objects are required to display evidence of bridges or asymmetries to be classified as mergers.

¹⁰ Trimmed (or truncated) means are robust estimators of central tendency, and it is less sensitive on the outliers than the mean. Trimmed means are derived by calculating the mean after discarding parts at the high and low ends of a probability distribution. In our case, the distribution is defined by the number of mergers obtained for each sample by each of the classifiers, and we reject 10% at both ends. Note that a 50% trimmed mean would correspond to the median.

Table 5
Observed Merger Fractions (Trimmed Means) For the $z > 1$ Samples

| Sample | Sample Size | Merger Fraction |
|---------------------|-------------|-----------------|
| H _z 3C | 11 | 100% |
| H _z LLRG | 8 | 88% |
| LPTy2AGN | 26 | 38% |
| HPTy2AGN | 9 | 33% |
| Bright Galaxies | 45 | 27% |
| Faint Galaxies | 46 | 20% |
| RL (3C+LLRG) | 19 | 95% |
| RQ (HP+LPTy2AGN) | 35 | 37% |

in the isophotes of the galaxies, in addition to the presence of small companions.

The observed merger fraction in the radio-loud samples (H_z3C and H_zLLRG) are clearly larger than those found for radio-quiet and non-active galaxies. In Section 4, we test this result using careful statistical analysis.

3.1. On the Impact of Different Sensitivities on the Merger Classification

The goal of this work is to identify merging systems in samples of objects that were observed as part of different surveys or observing programs. All of the images were taken using the WFC3-IR camera. Its extremely high sensitivity and spatial resolution allows us to detect low surface brightness features that characterize recent merger events at $z \sim 1-2$ even in short (1 orbit or less) observations. However, for the sake of clarity, we report in Table 6 the 5σ surface brightness limits for the different surveys we use. To derive the limits we used the WFC3-IR Exposure Time Calculator (ETC). We assume a 2×2 pixel extraction area and a spectrum of an elliptical galaxy with a UV upturn to perform the conversion between F160W (used for the CANDELS observations) and F140W magnitudes. Although the CANDELS deep images we used for the radio-quiet samples and for the H_zLLRGs are deeper than all other data, we checked that the merger classification is not different if the shallower 3D-*HST* images are considered. The images show the very same features, irrespective of the redshift of the source. The faintest tidal structures are less prominent in the shallower images, but that does not significantly affect our classification. The short exposure times of the 3C snapshot survey are also sufficient to detect the faint features we are interested in, in the range of redshift of our sample, as shown by the fact that that sample has the greater observed merger fraction.

4. STATISTICAL ANALYSIS

The main goal of this work is to investigate if mergers are associated with AGN activity and if that plays a role in triggering such a phenomenon. Most importantly, we want to test whether different classes of AGNs (e.g., radio-quiet versus radio-loud, low versus high bolometric luminosity) are more likely to be triggered by merger than others. We also test the hypothesis that AGNs are no different than non-active galaxies.

We perform a set of statistical tests to compare the derived merger fractions for the five different samples described in Section 2. Throughout the paper, statistical tests are performed using different techniques in the *R* environment (R Core Team 2014).

We use the Bayesian version of the proportion test using *bayes.prop.test*, as part of the *Bayesian First Aid* package for *R* (Bååth 2014). In principle, Bayesian tests are more useful than classical proportion tests, since they provide an estimate of the relative frequency of success (e.g., Bolstad 2007). In this simplified version of the Bayesian tests, the priors are uninformative, i.e., a uniform distribution. This is suitable for our purposes, since we have no a priori knowledge of the distribution of mergers in each sample.¹¹

In Table 7 we list the relative frequencies of success for each sample, together with the 95% credible intervals.

By testing each sample against each of the others, we can firmly establish that the H_z3C has a larger merger fraction than both of the Ty2AGN samples ($P > 99.9\%$). The H_z3C merger fraction is also larger than that of the non-active galaxies (both bright and faint samples, $P > 99.9\%$). Furthermore, the H_zLLRGs are significantly more associated with mergers than the non-active galaxies ($P > 99.9$). All other tests are inconclusive.¹² However, these are very important results.

Furthermore, if we merge the two samples of $z > 1$ radio-loud objects and we test them against the radio-quiet AGNs, the result is extremely robust. The merger fraction in our sample of radio-loud AGNs is significantly higher than that in the radio-quiet sample. This is again a notable result, since the (Bayesian) merger fractions for the RL and RQ sample are 92% and 38%, respectively. As expected, the same result holds (with an even higher statistical significance) for the RL sample against the non-active (both bright and faint) galaxies, while the RQ sample does not show any statistically significant difference with respect to the non-active galaxies. It is particularly important to note the results for the samples that are matched in magnitude. On the one hand, the RL and the *bright* galaxy sample are different, and on the other hand, the RQ and the *faint* galaxy sample are statistically indistinguishable.

As a sanity check, to avoid possible biases from a selection made using near-IR magnitudes, we also used the smaller sample of *high-mass* non-active galaxies (see Section 2.5). In particular, given that we measure a merger fraction of $30\%_{-17\%}^{+19\%}$, the *high-mass* sample is statistically different from the H_z3C, with a Bayesian probability $>99.9\%$. On the other hand, the merger fraction in such a sample is statistically indistinguishable from those in both the *faint* and the *bright* samples of non-active galaxies.

Finally, we wish to point out that among the samples of radio-loud AGNs at $z > 1$ the large majority of the objects ($\sim 90\%$) appear to be associated with major mergers. On the other hand, for radio-quiet AGNs at $z > 1$, only $\sim 50\%$ of the observed mergers are major mergers. Note that this is only based on our qualitative visual classification of the mergers. A more careful classification would require 2D galaxy modeling and SEDs to derive stellar mass estimates for the galaxies

¹¹ We also perform a complete set of classical proportion tests using the *R* task *prop.test*. For these classical tests we reject the null hypothesis that the merger fractions in two samples are the same if the *p*-value is $p < 0.01$. Not surprisingly, the results are perfectly in agreement with the Bayesian relative frequencies. For the sake of clarity, here we only discuss in details the Bayesian results.

¹² For a 2-sample proportion test in classical statistics this means that we cannot reject the null hypothesis that the observed merger fractions in two samples are the same (p -value < 0.01). For our Bayesian treatment, this implies that the probability that one sample has a higher (or lower) merger fraction than the other is less than 99%.

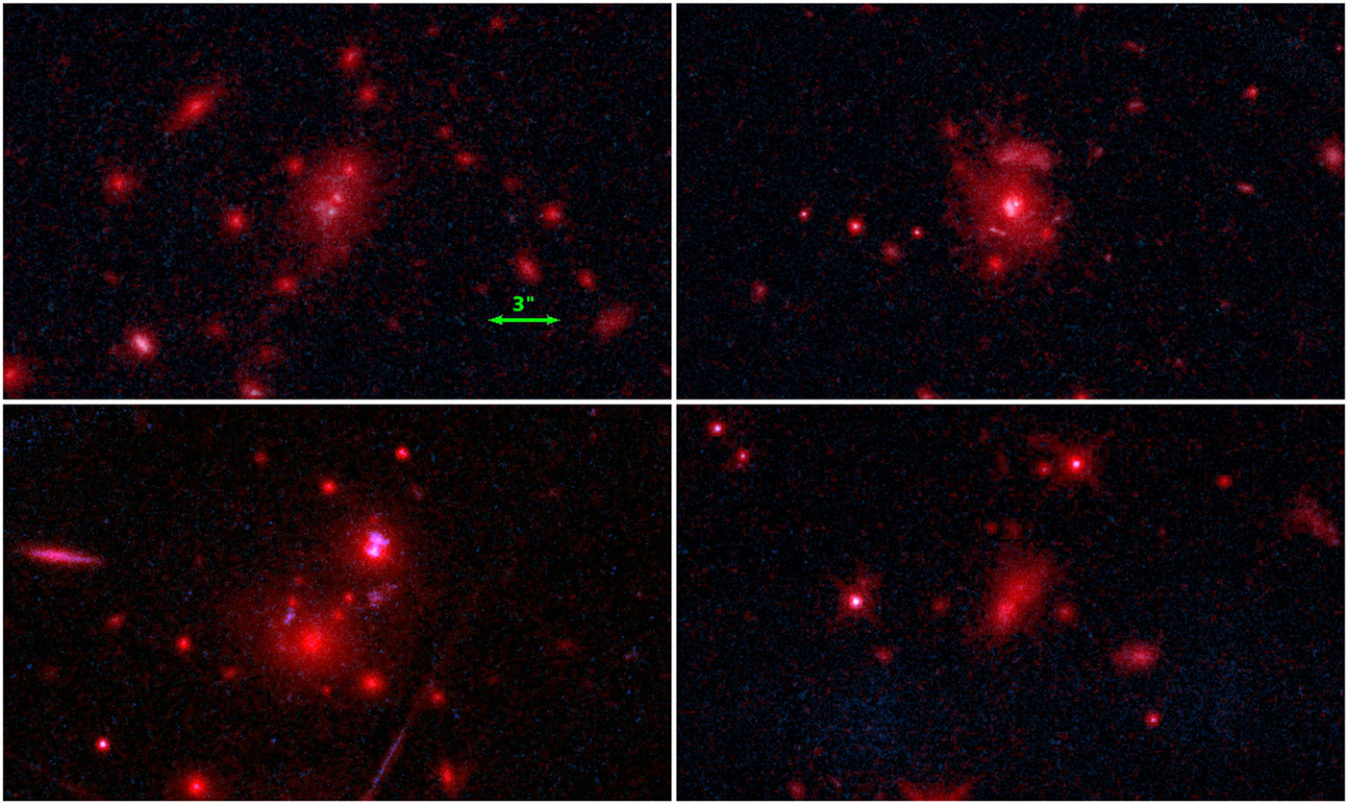


Figure 2. RGB images of four radio galaxies from the high- z 3CR sample showing clear evidence for recent or ongoing major merger. The objects are (from left to right, top to bottom) 3C 210, 3C297, 3C356, and 3C454.1. The *HST* WFC3-IR F140W image was used for the *R* channel. The WFC3-UVIS F606W image was used for both the *G* and *B* channels. North is up, East is left. Data from B. Hilbert et al. (2015, in preparation).

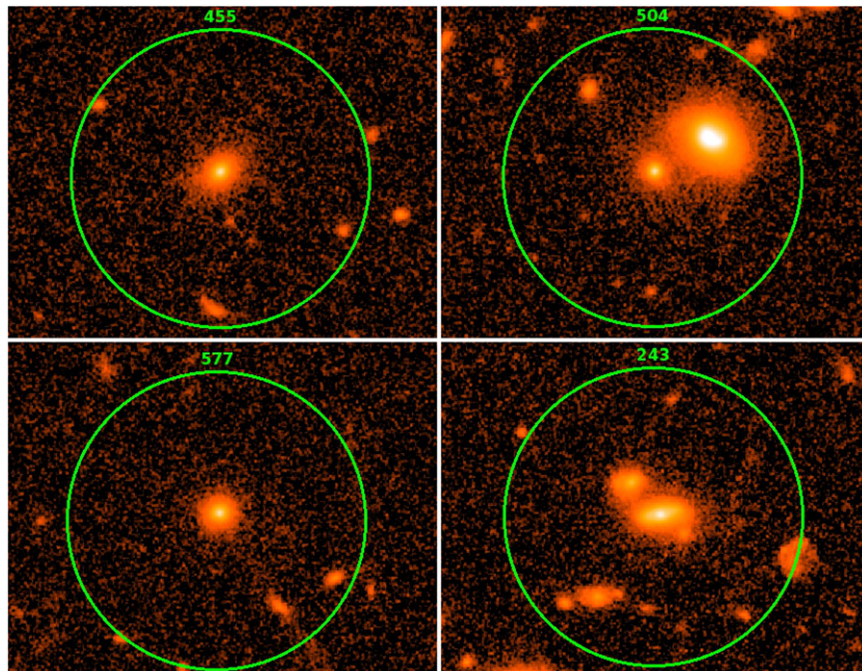


Figure 3. Four examples of the morphologies observed among the $z > 1$ radio-quiet AGNs. In the top panels, we show two LPTy2AGNs. A non-merger and a merger are shown on the left and on the right, respectively. In the bottom panels, the same is shown for two HPTy2AGNs. The circles are 6 arcsec radius, which correspond to ~ 50 kpc at the redshift of the objects. Images are from CANDELS (Grogin et al. 2011; Koekemoer et al. 2011, *HST*/WFC3/F160W).

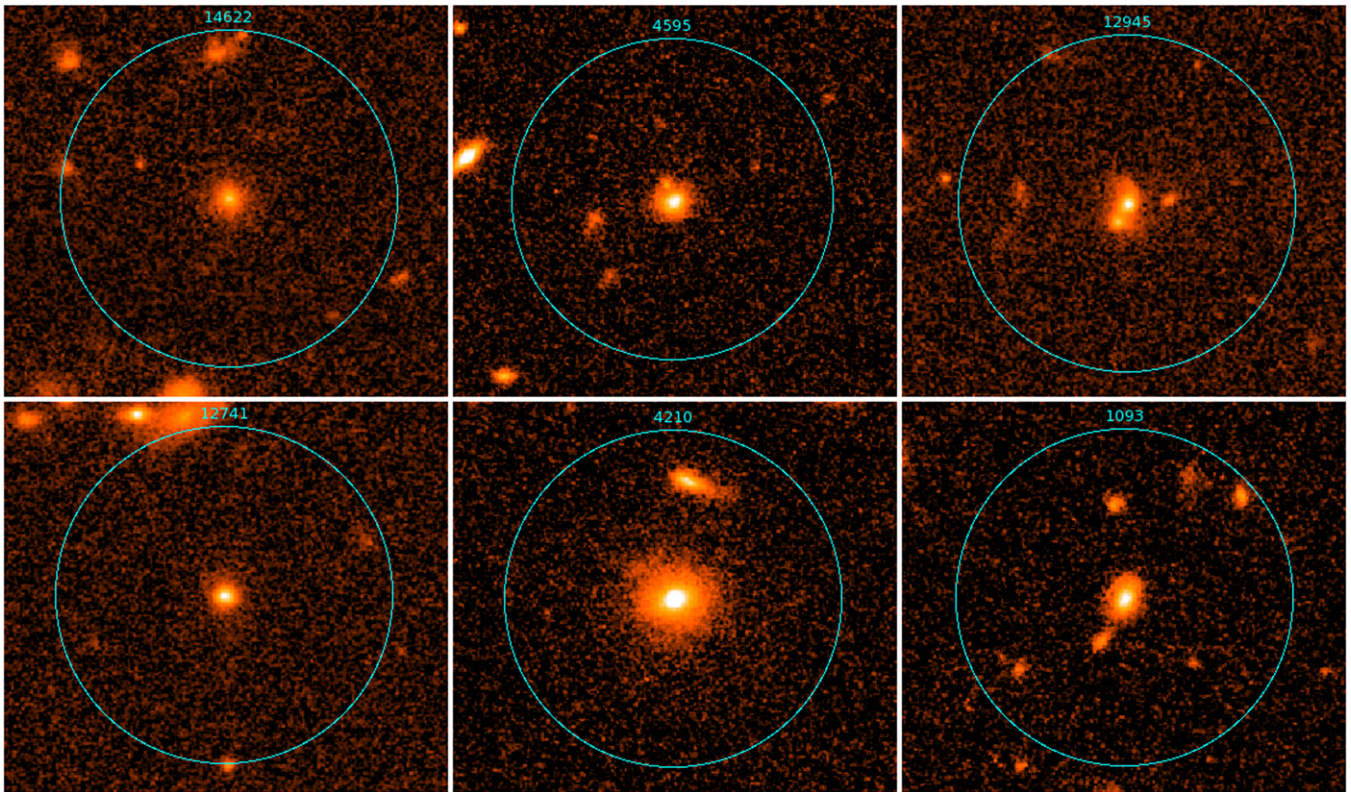


Figure 4. Six examples of non-active galaxies from our $z > 1$ sample. Both in the top and bottom rows, objects that are unanimously classified as non-mergers or mergers are shown in the left and right panels, respectively. Objects with mixed classification are shown in the middle panels. The circles are 6 arcsec radius, which correspond to ~ 50 kpc at the redshift of the objects. Images are from 3D-*HST* (Giavalisco et al. 2004; Brammer et al. 2012; Skelton et al. 2014, *HST*/WFC3/F140W).

involved in each merger, which is beyond the goals of this work.

4.1. Lower Redshift Samples of Radio Loud AGNs

One important goal of this work is to establish whether the merger fraction for radio-loud AGN depends on either redshift or luminosity. In order to test if that is the case, we used additional lower redshift samples, for comparison with the $z > 1$ data.

McLure et al. (2004) observed a sample of 41 intermediate ($z \sim 0.5$) radio galaxies with *HST* and WFPC2 (GO 9045, P.I. Willott). The sample is taken from four different complete catalogs, spanning about 4 dex in radio power. The four catalogs are all complete, flux limited and radio selected at low frequencies. The sample includes objects from the 3CRR, 6CE, 7CRS, and the TexOx-1000 (TOOT sample, hereinafter) (McLure et al. 2004, and references therein). The redshift range spanned by the objects observed with WFPC2 is between $z = 0.40$ and 0.59 . We will refer to these galaxies as the Willott sample throughout the paper.

For these objects, we retrieved the *HST* data from the MAST and we reduced them using *Astrodrizzle* (Fruchter et al. 2012). We then classify the objects between mergers and non-mergers, since no classification was provided in the original paper by McLure et al. (2004), and for consistency with the other samples. Note that the filter used for these observations (F785LP) provides images at ~ 5300 Å in the rest frame. This is similar to the rest frame wavelength of the WFC3-IR observations for the $z > 1$ samples described above. In Table 8 we report the merger fractions for this sample. The merger

fractions are statistically compatible with those for the radio-loud samples at higher redshifts.

At even lower redshifts, we use the observations of the 3CR sample with $z < 0.3$ taken with *HST*-NICMOS (program SNAP10173) and the F160W filter (Madrid et al. 2006). Although these observations are in the rest-frame IR, they are more suitable for our purposes than the optical data of the same sample taken with WFPC2 (de Koff et al. 1996; Martel et al. 1999) because the NICMOS images are significantly deeper. For this sample, we consider the results published by Floyd et al. (2008). These authors classified all of the objects in mergers, pre-mergers, tidal-tails, major, and minor companions. The field of view was covered by NIC2 is $19\frac{1}{2} \times 19\frac{1}{2}$, which corresponds to 50×50 kpc² at the median redshift of the sample. They found that 89 out of 101 objects fall into at least one of these categories. This corresponds to a merger fraction of 0.88, with a Bayesian 95% credible interval [0.81–0.94]. If we exclude objects with only *minor* companions (i.e., ≥ 1 mag fainter than the radio galaxy host, as defined by Floyd et al., 2008), the fraction is reduced to 0.76 with a Bayesian 95% credible interval [0.68–0.84].

Since the observations are not homogeneous, these two lower redshift samples are only considered here for comparison. However, we do not base our conclusions on these samples only.

5. DISCUSSION

The main result of this work is that the samples of radio-quiet and radio-loud Type 2 AGNs at $1 < z < 2.5$ have different merger fractions. We showed that there is clear

Table 6
Surface Brightness Limits

| Survey or <i>HST</i> Prog. ID | Sample | <i>HST</i> Camera/Filter | 5σ Surface Brightness Limit μ_{F140W} (AB mag arcsec ⁻²) | Sensitivity AB mag |
|-------------------------------|-------------------|--------------------------|--|-----------------------|
| SNAP-13023 | Hz3C | WFC3/F140W | 23.9 | 25.8 |
| CANDELS wide | RQ and HzLLRG | WFC3/F160W | 24.1 | 26.5 |
| CANDELS deep | RQ and HzLLRG | WFC3/F160W | 25.6 | 27.2 |
| 3D- <i>HST</i> | non-active | WFC3/F140W | 24.1 | 26.2 |
| GO-12866 | HzLLRG | WFC3/F160W | 25.0 | 26.7 |
| Low- <i>z</i> Samples | | | | |
| GO-9045 | 3CRR,6C,7C,TOOT | WFPC2/F785LP | 20.7 | 24.9 |
| SNAP-10173 | 3CR ($z < 0.3$) | NICMOS/NIC2/F160W | 22.5 | 24.3 |

Note. The 5σ limits are estimated using the WFC3-IR ETC and assuming a 2×2 pixel extraction region. In column 4 we report the limit surface brightness for each data set converted to the WFC3-IR F140W filter to allow for an easy comparison between the different surveys. An elliptical galaxy spectrum with UV eum redshifted to the appropriate redshift for each sample was used for the conversion between the two WFC3 filters. RQ in the samples column refers to both the LP and HPTy2AGN samples. For the low redshift samples (GO9045 and SNAP10173) we used *synphot* to convert magnitudes to the WFC3 filter system. In column 5 we report the 5σ image sensitivities calculated for point sources in each of the bands used for the observations.

Table 7
Estimated Bayesian Probabilities For the $z > 1$ Samples

| Sample | Merger Fraction | 95% Credible Interval |
|------------------|-----------------|-----------------------|
| Hz3C | 94% | 0.78–1.00 |
| HzLLRG | 82% | 0.57–0.99 |
| LPTy2AGN | 39% | 0.22–0.57 |
| HPTy2AGN | 36% | 0.11–0.64 |
| Bright Galaxies | 27% | 0.15–0.40 |
| Faint Galaxies | 20% | 0.10–0.33 |
| RL (3C+LLRG) | 92% | 0.78–1.00 |
| RQ (HP+LPTy2AGN) | 38% | 0.23–0.54 |

Table 8
Estimated Bayesian Probabilities For the $z < 1$ Radio-loud AGN Samples

| Sample | Size | Merger Fraction | 95% Credible Interval |
|-----------------------------|------|-----------------|-----------------------|
| Willott Samples | | | |
| 3CRR | 13 | 74% | 0.53–0.94 |
| 6CE | 7 | 68% | 0.38–0.93 |
| 7CRS | 9 | 65% | 0.37–0.89 |
| TOOT | 12 | 65% | 0.39–0.87 |
| Full Sample | 41 | 70% | 0.56–0.83 |
| Low Redshift Radio galaxies | | | |
| $z < 0.3$ 3CR | 101 | 88% | 0.81–0.94 |

statistical evidence that the radio-loud AGNs almost always reside in environments where mergers are undergoing, or that recently happened. As discussed below, this is independent of the radio (or bolometric) power of the AGN, and it is statistically compatible with merger fractions as high as $\sim 100\%$.

The sample with the highest observed merger fraction is the $z > 1$ 3CR. In principle, this sample could be biased, since *HST* only imaged $\sim 35\%$ of the radio galaxies with $z > 1$ included in the 3CR catalog. However, it is important to note that the observations were performed as part of an *HST* SNAPSHOT program. In SNAP programs, targets are randomly selected based on the availability of gaps in the *HST* schedule. Therefore, there was no a priori knowledge of the properties of the observed targets with respect to the complete sample.

But since the observed sample is small, it is still possible that we ended up picking a large number of objects in mergers only by chance. In the following we briefly discuss such an issue. For example, we could, in principle, assume that the original population is composed by $\sim 50\%$ of mergers and 50% of non-mergers, similarly to what is observed in our sample of non-active galaxies. We can test the probability of obtaining a sample of 12 mergers, randomly extracted from the complete sample of 34 radio galaxies included in the 3CR catalog with $z > 1$. The selection of the 3CR catalog only covered part of the sky (decl. $> -10^\circ$). Therefore, we should correct for the area coverage to obtain the total number of radio sources (i.e., 58 radio galaxies). The binomial probability of obtaining 12 mergers out of 12 observed is extremely small ($P = 2 \times 10^{-4}$). However, when objects are randomly drawn from a sample without replacement, the Hypergeometric distribution must be used instead of the binomial. In that case, the probability of obtaining 12 mergers out of 12 observed, from a population of 58 objects in which 50% of the objects are mergers is $P = 5.8 \times 10^{-5}$. Note that if the merger fraction in the complete sample is higher than 72% , then the (hypergeometric) probability of obtaining 12 mergers is $P > 0.01$. Since that corresponds to the significance level we set for all of the statistical tests, we can state that we cannot completely rule out that the merger fraction in the 3CR is as low as $\sim 72\%$. Interestingly, this is similar to the lower value of the credible interval given by the Bayesian analysis for this sample (see Table 7). The only other selection bias that might affect our sample is the Eddington (1913) bias. However, that would have the effect of lowering the actual number of sources in our sample, and that in turn would lower the probability of the hypergeometric distribution.

Therefore, we conclude that even if the number of 3CR galaxies observed at $z > 1$ is small, the probability that the observed merger fraction is overestimated because of any selection bias is extremely small.

5.1. Radio-loud Samples: No Trends with Redshift and Luminosity

In this section we discuss the results we obtained for the different radio-loud samples. It is in fact particularly interesting to investigate whether the merger fraction in these objects may

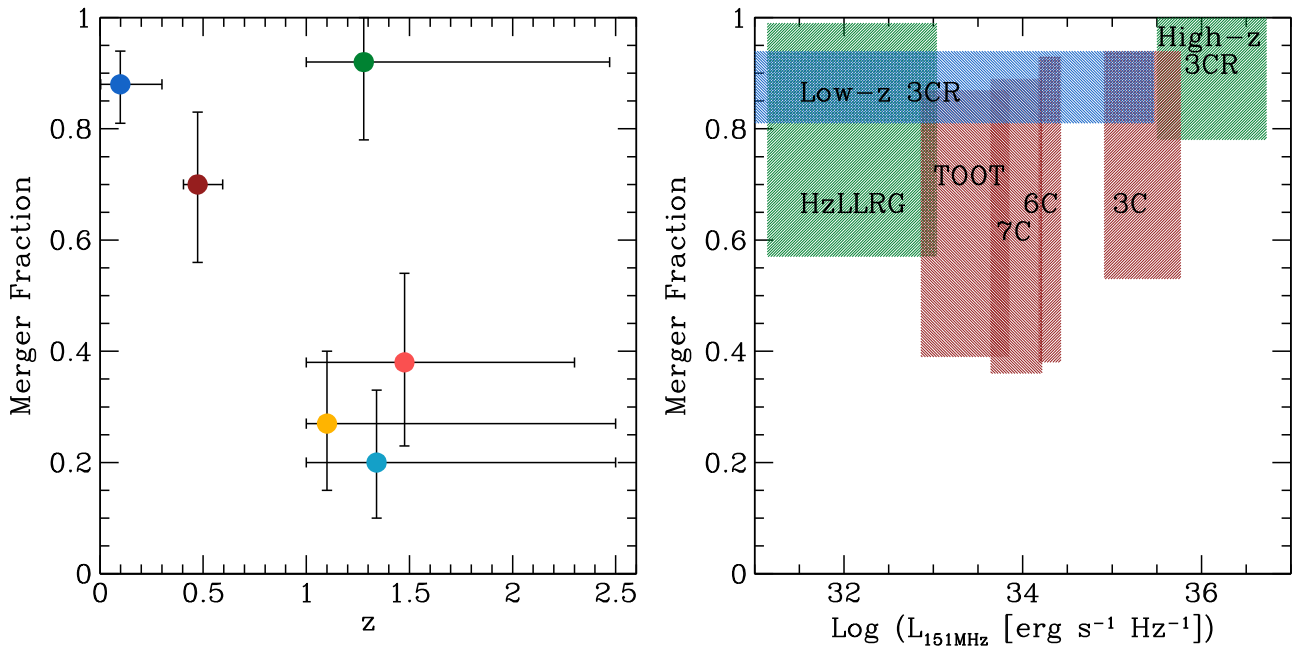


Figure 5. Left: merger fraction vs. redshift for the samples of radio-loud and radio-quiet AGNs, and for non-active galaxies. The coordinates of the filled dots are the median redshift of each sample, and the Bayesian merger probability. The error bars show the range of redshift spanned by each sample and the Bayesian 95% credible intervals for the merger probability. The high- z radio-loud sample (green dot) corresponds to the 3CR at $z > 1$ merged with the HzLLRG sample to improve the statistics. The radio-quiet Ty2 AGN samples at $z > 1$ are also merged (light red). The bright and faint samples of non-active galaxies are plotted in yellow and cyan. The Willott sample (3CR, 6CE, 7CRS, and TOOT samples at $z \sim 0.5$) is in red. The blue dot represents the 3CR sample with $z < 0.3$. Right: merger fraction vs. radio luminosity at 151 MHz for the radio-loud samples. In this panel, the Willott samples (here marked as TOOT, 6C, 7C, and 3C) and the high- z radio-loud samples (Hz3CR and HzLLRG) are plotted separately. The color code is the same as for the left panel.

depend on, e.g., redshift, luminosity, or on the original criteria for each sample selection. However, while the statistical analysis clearly shows that radio-loud objects are almost all associated with mergers, one important *caveat* is that the samples are small. This is particularly true for the radio-loud samples (except for the low- z 3CR), but also for the high- z radio-quiet comparison sample. Unfortunately, this prevents us from drawing statistically firm conclusions on any possible trend between the different samples of radio galaxies. For example, we cannot determine whether the HzLLRG’s are less likely to be associated with mergers than the Hz3C’s even if the observed fraction is lower in the former than in the latter. Similarly, we cannot determine whether each of the samples at $z \sim 0.5$ that compose the Willott sample behave differently, for example as a result of their different radio power.

However, it is interesting to consider radio-loud samples grouped by redshift bin. We can thus compare the merger fractions for the low- z 3CR, the whole Willott sample (TOOT+7CRS+6CE+3CRR), and the high- z objects (3CR+HzLLRG). In Section 4 we showed that we find no statistical evidence that the observed merger fractions are different for any of those groups. Therefore, while we wish to stress that this does not imply that they are the same, we can conclude that the data show no evidence for a redshift evolution. By comparing the 95% Bayesian credible intervals, we can also conclude that the merger fractions do not differ by more than $\sim 20\%$. Since the samples are well separated in radio luminosity, it is straightforward to perform a similar analysis for samples grouped by radio luminosity, and conclude that the merger fraction in low- and high-power samples does not differ by more than 20%. This is a notable result, since these samples

are separated by more than 4 dex in radio power, and span a wide range of redshift (see Figure 1).

In Figure 5 we show the Bayesian 95% credible intervals for each of the groups of radio-loud objects plotted against the redshift (left panel) and radio luminosity (right panel) range spanned by each group. In the left panel (merger fraction versus redshift) we also include the radio-quiet AGNs and the two samples of non-active galaxies. The radio-quiet AGNs and the non-active galaxies are not plotted in the right panel, since any trends with the radio power would be irrelevant. In fact, the origin of radio emission in radio-quiet AGNs is still debated, as it could be either thermal or non-thermal, and a possible contribution from starbursts could not be excluded at the lowest luminosities. Starbursts are instead the most likely origin for the radio emission in non-active galaxies. These objects would lie on the bottom-left of the figure in the right panel, but any correlation with the merger fraction would be meaningless. As it is clear from the figure (left panel), the only group of radio-loud AGNs that is still marginally compatible with the radio-quiet samples is the Willott sample. However, this might be due to the fact that the images were taken with WFPC2, which was significantly less sensitive than WFC3-IR. In Table 6 we report the limit magnitude estimated using the WFPC2 ETC, and converted to the F140W filter using *synphot* to allow an easier comparison with the WFC3 observations. The value $m_{F140W} = 20.7$ mag arcsec⁻² was derived using an elliptical galaxy spectrum redshifted to $z = 0.5$. As a result of that, some images might not show faint surface brightness structures such as e.g., asymmetries or tidal tails, which might lead us to misclassify some of the objects as non-mergers. Deeper images with WFC3 or with ACS in the I band should be taken in order

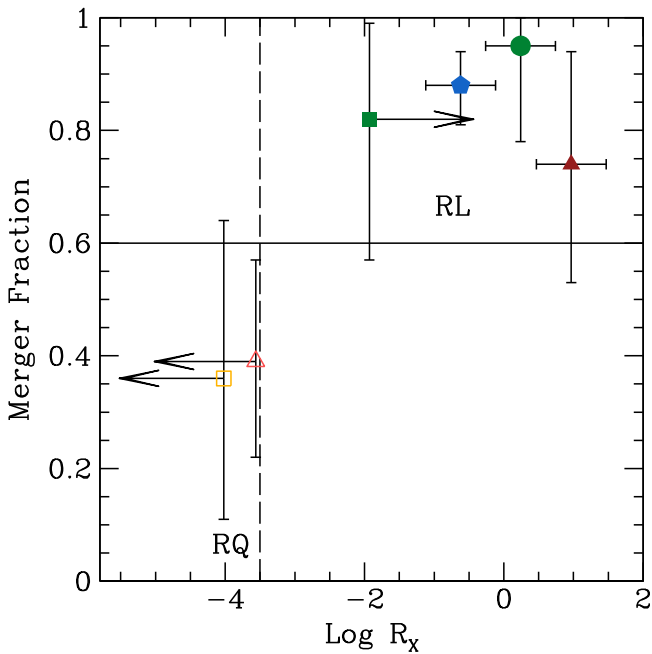


Figure 6. Merger fraction vs. average radio-loudness parameter R_x for the different AGN samples. Filled symbols are the radio-loud samples, empty symbols are radio-quiet. The Hz3C sample is plotted as a circle, the HzLLRG is the square (lower limit), Willott’s 3CRR is the triangle, and the low- z 3CR is the pentagon. For the radio-quiet samples (empty symbols) the LPTy2AGN sample is the triangle, and the HPTy2AGN is the square. The dashed line represents the radio-loudness threshold for PG QSOs (Terashima & Wilson 2003). The solid line marks the 60% merger fraction that appears to roughly separate radio-loud and radio-quiet samples. Color code is the same as for Figure 5.

to achieve a more reliable estimate of the merger fraction in the Willott sample.

The right panel of Figure 5 shows the merger fraction for each sample, against radio power at 151 MHz.¹³ Here we plot the Willott samples separately, since they belong to different luminosity bins. The low- z 3CR span a large range in radio power. Most of these 3CR objects are confined to the lower luminosity bin, as it is clear from Figure 1. As noted above, except for the low- z 3CR for which the merger fraction is much better constrained, the number statistics is small and the error on the merger fraction is large. However the figure clearly shows that all of the samples are located in the upper part up the diagram, and that no trend with radio power is visible.

Finally, in Figure 6 we show the merger fraction against the radio-loudness parameter R_x . In order to represent the average value of R_x for each sample, we calculated average values for both the radio and the X-ray luminosities (see the caption for references). The data are very uncertain, since the information is extremely sparse. This especially holds for the X-ray data of the Hz3C and the Willott sample, while most of the HzLLRG only have upper limits in the X-ray band, so the radio-loudness of the HzLLRGs is represented as a lower limit. Note that $\sim 20\%$ of the radio-quiet objects are detected in the radio band. The value of R_x for the radio-quiet samples is thus calculated using the average radio luminosity for the detected objects, and the points in the figure are shown as upper limits for the radio-loudness parameter. For all other samples, to be safe, we

assume uncertainties up to $\sim \pm 0.5$ dex in R_x . This is reasonable considering the uncertainties in the X-ray luminosity and the range of radio and X-ray luminosity spanned by the objects.

This plot summarizes the main result of this work, i.e., that radio-quiet sources are systematically associated to smaller merger fractions (and they are located in the lower-left side of the figure), while radio-loud AGNs are unambiguously associated with mergers (and they are located in the upper-right side of the figure).

5.2. Comparison with Other Recent Results

Our results basically agree with the findings of Ramos Almeida et al. (2012) and Ramos Almeida et al. (2013). Those studies focus on samples of relatively low-redshift ($z < 0.7$) sources with deep ground based observations. These authors found that the large majority ($\sim 80\%$) of radio-loud objects show disturbed morphologies, and they also reside in dense environments. However, the parameter space covered by those papers is limited to luminous low-redshift objects, while our work spans a significantly larger range both in redshift and luminosity. The same group also studied a sample of 20 Type 2 quasars (Bessiere et al. 2012) that includes at least two RLQSOs, based on their location in the $L_{5\text{ GHz}}$ versus $L_{[\text{O III}]}$ plane (Xu et al. 1999). As expected in light of our results, both RLQSOs are associated with mergers. The merger fraction in the full sample is as high as 75%. If we only exclude those two sources that exceed their definition of radio-loudness, the observed merger fraction among the remaining radio-quiet objects is still quite large (72%). While this might appear in disagreement with our measured fraction for the RQAGNs, the uncertainty on the value found by these authors is large, as a result of the small number statistics (13 possible mergers out of 18 objects). Since the samples are small, we cannot reject the null hypothesis that a 72% merger fraction for that sample is different from the fraction measured in our sample of RQAGNs.

One of the major points here is that we showed that there is no evidence for a trend with luminosity, at least for the radio-loud samples. This is apparently at odds with the results of Treister et al. (2012), where only the most powerful samples appear to predominantly reside in merging systems. However, it is interesting to briefly discuss their work in the light of our results. Two samples show a significantly greater merger fraction than any other samples treated in that work. Those are the sample of dust-reddened Type 1 QSOs of Urrutia et al. (2008) and the Bahcall et al. (1997) sample of Type 1 QSOs. The former is most likely biased in favor of a high merger fraction, because of the nature of those obscured quasars. The latter, instead, is more interesting. Of the 20 QSOs observed with *HST* by Bahcall et al. (1997), 14 are radio-quiet and 6 are radio-loud. All of the 6 RLQSOs are apparently merging or show irregular features that might be explained with a merger, in agreement with our results. Thus if we only limit the analysis to the RQSOs, the fraction of mergers is $\sim 50\%$, in agreement with our findings. Therefore, we argue that the high fraction of mergers in the full Bahcall sample (65%) could in principle be explained, in light of our results, by the fact that a significant fraction of the objects are radio-loud.

¹³ Measurements at radio frequencies different from 151 MHz were converted to the reference wavelength using a spectral index $\alpha = 0.8$ and $F_\nu \propto \nu^{-\alpha}$.

6. IMPLICATIONS FOR THE ORIGIN OF RADIO-LOUDNESS

Our results show that radio galaxies are unambiguously associated with mergers, independently of redshift and luminosity, while radio-quiet AGNs at $z > 1$ are indistinguishable from normal galaxies in the same redshift range. This result may have profound implications for our understanding of the mechanisms that enable the production of powerful relativistic jets from supermassive BHs. In fact, such a strong connection between mergers and radio-loud AGNs may be a clue for a direct link between these two phenomena.

The central question here is whether mergers may provide, or at least substantially contribute to the physical conditions that ultimately enable the formation of jets in RLAGNs.

6.1. Not All Mergers May Generate an RLAGN

First of all, we should point out that most mergers do not generate an RLAGN. This is clear from the fact that a fraction of non-active galaxies at $z > 1$ are seen to be merging, but they show no signs of radio-loud activity. If there is an association between these two phenomena, it is not a univocal cause/effect relationship. Based on our results, the same also holds for radio-quiet AGNs since a fraction of those are associated with mergers. Thus, we conclude that mergers are unrelated to radio-quiet AGNs or, alternatively, only a fraction of those may be triggered by mergers. However, it is worth noting that our definition of merger includes objects that still have to merge as well as objects for which the signs of a past merger are somehow still visible. Therefore, the timescale during which we observe a merger is probably of the order of at least $\sim 1\text{--}2$ Gyr (e.g., Di Matteo et al. 2005). The time scale for radio-loud activity is most likely significantly shorter ($\sim 10^7\text{--}10^8$ years). Therefore, we cannot exclude that some of the non-active galaxies that we observe in a merger phase are turned-off radio-loud AGNs, or, alternatively, they still have to be turned-on. Summarizing, we believe that not all mergers may directly generate a radio-loud AGN. Below we discuss a few possible conditions for a merger to trigger RLAGN activity.

6.2. Conditions for Mergers to Trigger RLAGNs

We argue that when certain conditions are met, mergers may trigger radio-loud nuclear activity. What we ultimately wish to know is what those conditions are. An important piece of information here is that the association between mergers and RLAGNs is robustly established at all redshifts. While both recent simulations and observations show that the galaxies merger rate increases with redshift (e.g., Conselice et al. 2003; Hopkins et al. 2006; Lotz et al. 2011; Rodriguez-Gomez et al. 2015), our results show that there is no evidence that the merger fraction for RLAGNs is higher at higher z . Of course, this should be confirmed through the analysis of larger samples that may better constrain the merger fractions and highlight any possible trends with redshift. But even if the uncertainties remain large with the present samples, the existence of such a tight relationship between the two phenomena means that somehow an RLAGN needs a merger (at all redshifts) in order to manifest itself. The predominance of major mergers among our radio-loud samples (at least at $z > 1$) that is apparent from visual inspection needs to be confirmed through a more quantitative analysis. However, this may imply that one of the conditions that must be met in order to trigger an RLAGN is

that the merger needs to be between two galaxies (and thus between two BHs) of similar mass. It is well known that radio galaxies are ubiquitously associated with very massive hosts ($\gtrsim 10^{10\text{--}11} M_{\odot}$, e.g., Best et al. 2005) and high-mass SMBH ($\gtrsim 10^8 M_{\odot}$, Laor 2000; Dunlop et al. 2003; Chiaberge & Marconi 2011; Best & Heckman 2012). Therefore, we expect those major mergers to involve high-mass objects only.

6.3. How do Mergers Affect the Central SMBHs?

Understanding the details of this issue is central to our future work on the subject, but it is beyond the scope of this paper. However, we can build on our results and speculate on a possible scenario. One of the effects of mergers is to lower the specific angular momentum of the gas in the galaxy, and thus to drive the gas toward the center (e.g., Hernquist 1989; Hopkins & Quataert 2011). While this may naturally happen in gas-rich mergers, as those observed in our high- z 3CR sample (e.g., Barthel et al. 2012; Tadhunter et al. 2014; Podigachoski et al. 2015), the hosts of low-redshift radio galaxies (in particular those of low radio powers) are often relatively gas-poor systems. Therefore, this effect may play a role at higher redshifts, but it is very unlikely to be the ultimate cause of radio-loud activity in general. Furthermore, tidal effects happen in all mergers, thus merger events should affect both RQ and RL AGNs at the same level, contrary to our results.

Another effect of mergers is to alter the spin and the mass of the central BH. That can be achieved in two ways, i.e., either via accretion, or via BH–BH merger (e.g., Volonteri et al. 2013). The former implies that a large amount of gas is driven toward the central region of the galaxy, for a significant amount of time. If the accretion of matter is coherent, i.e., if the flow of matter occurs at a fixed angular momentum axis, that ultimate leads to spinning-up the BH. On the other hand, if accretion results from multiple merger events that drive the matter toward the BH from different directions, the BH is spinned-down. In any case, as already pointed out above, the expected amount of gas in major mergers (at least at low redshifts) is probably too small to alter the BH spin significantly in these objects.

In the case of BH–BH merger, the two BH coalesce and the resulting object has increased mass and, in most cases, a lower spin per unit mass. But there are scenarios in which those events lead to the opposite result. For example, it has been shown that a single major BH–BH merger, where the ratio between the masses of the two involved BHs approaches unity, may generate a spinning BH, even if the two merging BH are initially not spinning (Hughes & Blandford 2003; Baker et al. 2006; Li et al. 2010; Giacomazzo et al. 2012; Schnittman 2013, for a recent review). However, current simulations are unable to reproduce BH with dimensionless spin parameter greater than ~ 0.94 as a result of BH–BH mergers alone (Hemberger et al. 2013).

6.4. The Role of Rapidly Spinning BHs

According to the so-called spin paradigm (Blandford et al. 1990, p. 97; Wilson & Colbert 1995), radio-loud AGNs are associated with rapidly spinning BHs, while BHs in radio-quiet AGNs are expected to spin less rapidly. Those major mergers that result in rapidly spinning BHs may provide the link between our observations and the physics behind the RLAGNs phenomenon as a whole. Clearly, the objects that we

are seeing in a pre-merger phase, or the very few ones that are associated with a minor merger, do not fit the above scheme. In those cases, we must assume that another major merger event happened in the recent past. This does not seem unreasonable, since all of these objects lie in over-dense environments, but it should be proven by finding the signatures of that previous merger.

In a framework in which BHs are spun up by major BH–BH mergers, we expect a range of resulting spin values. Therefore, it is possible that different radio morphologies (and radio powers) are associated with different BH spin levels. For example, only the BHs that spin more rapidly might be able to produce the most relativistic jets, in a framework in which the jet is powered by energy extracted from the rotating BH (e.g., Blandford & Znajek 1977; McKinney et al. 2012; Ghisellini et al. 2014). Such a scenario has been explored for X-ray binaries jets, so far leading to contrasting results (e.g., Fender et al. 2010; Narayan & McClintock 2012; Russell et al. 2013; Gardner & Done 2014). It is interesting to note that Fanidakis et al. (2011) were able to reproduce the RL and RQ AGN populations in the context of galaxy evolution. Their model is based on a scheme that includes a bimodal BH spin distribution mainly caused by the combination of accretion of matter onto the BH and by the different type of mergers that galaxies of different stellar mass undergo.

As pointed out in the previous section, BHs could also be spun-up by merger-triggered accretion. Such a mechanism could in principle account for our observations of mergers at $z > 1$, but only if those are gas-rich mergers. However, it would not completely explain the origin of radio-loud activity in low redshift, gas-poor galaxies (see also the discussion in the next section).

6.5. Low Redshift Radio-loud AGNs

A scenario in which BH–BH mergers are directly implied in triggering radio-loud AGN activity seems to be supported by the observed properties of low-redshift RLAGN hosts. Capetti & Balmaverde (2006) and de Ruiter et al. (2005) showed that all radio-loud AGNs in their samples are hosted by core-galaxies, i.e., galaxies that show a flat radial brightness profile in the central regions. While this analysis is clearly limited to very low redshifts ($z \lesssim 0.1$), where the core radius can be resolved in *HST* images, and to objects that are not affected by significant amounts of dust in the central kiloparsecs, it very clearly shows that there is a strong connection between the presence of a *core* profile and RL activity. Interestingly, one of the most likely explanations for the presence of core profiles is related to a major BH–BH mergers, in which the binary BH formed during the merger ejects stars from the central regions before the two BHs coalesce (e.g., Graham 2004; Merritt 2006). While the direct physical connection between such a phenomenon and radio-loud activity is still a matter of debate (see e.g., Chiaberge & Marconi 2011), it provides one more piece of evidence that major mergers and radio-loud AGNs are strictly connected.

7. CONCLUSIONS

We derived the merger fraction in samples of $z > 1$ Type 2 RLAGNs, Type 2 RQAGNs, and non-active galaxies. We establish that the RLAGNs are unambiguously associated with mergers ($92\%_{-14\%}^{+8\%}$), while only $38\%_{-15}^{+16}$ of the RQAGNs show

evidence for a merger. Non-active galaxies are statistically indistinguishable from the RQAGNs. The comparison with lower redshift samples shows that there is no evidence for the fraction of mergers in RLAGNs to be dependent on either redshift or AGN luminosity.

Mergers are directly involved in triggering radio-loud activity at all redshifts. We speculate that the galaxy mergers we observe at $z > 1$ are responsible for spinning up central BHs possibly through mergers of high-mass BHs.

It will be extremely important to study the BH mass distribution in samples of merging galaxies of different type and to determine whether the BH mass and the merger types are related to different type of activity.

Not all galaxy mergers in our RL samples appear the same to visual inspection. It would be important to firmly assess the ratio between major and minor mergers at different redshifts, and radio power. The images in this work show that a larger fraction of objects are in a phase of ongoing- or post-major merger in higher redshift samples than in the lower redshift counterparts (see also Floyd et al. 2008). The different *HST* cameras used not only sample different rest-frame wavelengths (near-IR at low- z and optical at $z > 0.4$), but they also have significantly different sensitivities. It is extremely hard to detect post-merger signatures such as e.g., faint tidal tails in the intermediate redshift samples imaged with WFC2. Those features may lie outside the field of view in the NICMOS images at low redshift. The only redshift range that is covered with homogeneous observations is between $z = 1$ and 2.5. Clearly needed is a homogeneous data set observed with *HST*-WFC3 or ACS at all redshifts.

Detailed studies of the mergers in our radio-loud samples using integral field spectroscopy, combined with deep high resolution imaging in the rest frame IR, should be used to study the kinematics of the mergers and measure a range of parameters such as dynamical masses and angular momenta. The imaging part of the project is feasible with WFC3, although at high redshifts the rest frame wavelengths sampled by such a camera are still within the optical bands. Dust obscuration may reduce the accuracy of the stellar mass measurements.

ALMA observations can trace the molecular gas involved in the mergers. It is important to study a large sample of these sources at different redshifts, to test whether different amounts of gas are driven toward the central SMBHs and whether that may affect the type of radio-loud nuclear activity. A comparison with the mergers observed in radio-quiet AGNs and in ULIRGs will elucidate the BH feeding mechanism in all of these sources, and relationships with AGN activity.

This work is limited to Type 2 AGNs because in Type 1 AGNs the nuclear light from the central QSO hampers morphological studies of the host galaxy. With a better knowledge of the WFC3 PSF, such a study is possible starting with the sample of 3CR QSOs at $z > 1$. Better results can be achieved using coronagraphic observations by Martel et al. (2003). While the coronagraphic mode is now available on *HST* only in STIS, the *James Webb Space Telescope* with NIRISS will allow us to image QSOs spanning a broader range of redshift. We hope to be able to study in detail both the structure and fueling mechanisms in Type 1 objects (see e.g., Ford et al. 2014).

In conclusion, our results clearly establish that RLAGNs are mergers. Conversely, based on the samples studied in this

paper, we did not find any statistical evidence that RQAGNs are related to merger events.

The authors wish to thank G. Zamorani, C. O’Dea, S. Baum, and A. Capetti for insightful comments and suggestions. We acknowledge W. B. Sparks and the *HST*-3CR collaboration for making the images of the $z > 1$ 3C radio galaxies available for this work. We are also indebted to M. Stiavelli and A. Mortazavi for helping out with the mergers classification. We are also grateful to the anonymous referee for their helpful comments that greatly improved the paper. This research has made use of the NASA/IPAC Infrared Science Archive, which is operated by the Jet Propulsion Laboratory, California Institute of Technology, under contract with the National Aeronautics and Space Administration. This work is based on observations taken by the CANDELS Multi-Cycle Treasury Program with the NASA/ESA *HST*, which is operated by the Association of Universities for Research in Astronomy, Inc., under NASA contract NAS5-26555. This work is based on observations taken by the 3D-*HST* Treasury Program (GO 12177 and 12328) with the NASA/ESA *HST*. Based on observations made with the NASA/ESA *HST*, obtained from the Data Archive at the Space Telescope Science Institute, which is operated by the Association of Universities for Research in Astronomy, Inc., under NASA contract NAS 5-26555.

REFERENCES

- Alexander, D. M., & Hickox, R. C. 2012, *NewAR*, 56, 93
- Bååth, R. 2014, in *UserR! 2014—the Int. R User Conf.*, Bayesian First Aid: A Package that Implements Bayesian Alternatives to the Classical *t-test Functions in R
- Bahecall, J. N., Kirhakos, S., Saxe, D. H., & Schneider, D. P. 1997, *ApJ*, 479, 642
- Baker, J. G., Centrella, J., Choi, D.-I., Koppitz, M., & van Meter, J. 2006, *PhRvD*, 73, 104002
- Balmaverde, B., Capetti, A., & Grandi, P. 2006, *A&A*, 451, 35
- Barthel, P., Haas, M., Leipski, C., & Wilkes, B. 2012, *ApJL*, 757, L26
- Bell, E. F., Naab, T., McIntosh, D. H., et al. 2006, *ApJ*, 640, 241
- Behroozi, P. S., Zhu, G., Ferguson, H. C., et al. 2015, *MNRAS*, 450, 1546
- Bessiere, P. S., Tadhunter, C. N., Ramos Almeida, C., & Villar Martín, M. 2012, *MNRAS*, 426, 276
- Best, P. N., & Heckman, T. M. 2012, *MNRAS*, 421, 1569
- Best, P. N., Kauffmann, G., Heckman, T. M., et al. 2005, *MNRAS*, 362, 25
- Best, P. N., von der Linden, A., Kauffmann, G., Heckman, T. M., & Kaiser, C. R. 2007, *MNRAS*, 379, 894
- Blandford, R. D., Netzer, H., Woltjer, L., Courvoisier, T. J.-L., & Mayor, M. 1990, *Active Galactic Nuclei*, Vol. 280 (Berlin, Heidelberg, New York: Springer)
- Blandford, R. D., & Payne, D. G. 1982, *MNRAS*, 199, 883
- Blandford, R. D., & Znajek, R. L. 1977, *MNRAS*, 179, 433
- Bolstad, W. M. 2007, *Introduction to Bayesian Statistics* (2nd ed.; New York: Wiley)
- Bonzini, M., Mainieri, V., Padovani, P., et al. 2012, *ApJS*, 203, 15
- Bonzini, M., Padovani, P., Mainieri, V., et al. 2013, *MNRAS*, 436, 3759
- Brammer, G. B., van Dokkum, P. G., Franx, M., et al. 2012, *ApJS*, 200, 13
- Capetti, A., & Balmaverde, B. 2006, *A&A*, 453, 27
- Cardamone, C. N., Urry, C. M., Damen, M., et al. 2008, *ApJ*, 680, 130
- Cardamone, C. N., van Dokkum, P. G., Urry, C. M., et al. 2010, *ApJS*, 189, 270
- Chiaberge, M., Capetti, A., & Macchetto, F. D. 2005, *ApJ*, 625, 716
- Chiaberge, M., & Marconi, A. 2011, *MNRAS*, 416, 917
- Colina, L., & de Juan, L. 1995, *ApJ*, 448, 548
- Condon, J. J., Cotton, W. D., Greisen, E. W., et al. 1998, *AJ*, 115, 1693
- Conselice, C. J., Bershady, M. A., Dickinson, M., & Papovich, C. 2003, *AJ*, 126, 1183
- de Koff, S., Baum, S. A., Sparks, W. B., et al. 1996, *ApJS*, 107, 621
- de Ruiter, H. R., Parma, P., Capetti, A., et al. 2005, *A&A*, 439, 487
- Di Matteo, T., Springel, V., & Hernquist, L. 2005, *Natur*, 433, 604
- Donoso, E., Li, C., Kauffmann, G., Best, P. N., & Heckman, T. M. 2010, *MNRAS*, 407, 1078
- Dunlop, J. S., McLure, R. J., Kukula, M. J., et al. 2003, *MNRAS*, 340, 1095
- Eddington, A. S. 1913, *MNRAS*, 73, 359
- Fanaroff, B. L., & Riley, J. M. 1974, *MNRAS*, 167, 31P
- Fanidakis, N., Baugh, C. M., Benson, A. J., et al. 2011, *MNRAS*, 410, 53
- Fender, R. P., Gallo, E., & Russell, D. 2010, *MNRAS*, 406, 1425
- Floyd, D. J. E., Axon, D., Baum, S., et al. 2008, *ApJS*, 177, 148
- Ford, K. E. S., McKernan, B., Sivaramakrishnan, A., et al. 2014, *ApJ*, 783, 73
- Fruchter, A. S., Hack, W., Dencheva, N., et al. 2012, in *American Astronomical Society Meeting Abstracts* 219, #145.15
- Gardner, E., & Done, C. 2014, *MNRAS*, 438, 779
- Ghisellini, G., Tavecchio, F., Maraschi, L., Celotti, A., & Sbarrato, T. 2014, *Natur*, 515, 376
- Giacconi, R., Zirm, A., Wang, J., et al. 2002, *ApJS*, 139, 369
- Giacomazzo, B., Baker, J. G., Miller, M. C., Reynolds, C. S., & van Meter, J. R. 2012, *ApJL*, 752, L15
- Gialalisco, M., Ferguson, H. C., Koekemoer, A. M., et al. 2004, *ApJL*, 600, L93
- Graham, A. W. 2004, *ApJL*, 613, L33
- Grogin, N. A., Kocevski, D. D., Faber, S. M., et al. 2011, *ApJS*, 197, 35
- Grogin, N. A., Koekemoer, A. M., Schreier, E. J., et al. 2003, *ApJ*, 595, 685
- Hawley, J. F., & Krolik, J. H. 2006, *ApJ*, 641, 103
- Heckman, T. M., & Best, P. N. 2014, *ARA&A*, 52, 589
- Heckman, T. M., Smith, E. P., Baum, S. A., et al. 1986, *ApJ*, 311, 526
- Hemberger, D. A., Lovelace, G., Lored, T. J., et al. 2013, *PhRvD*, 88, 064014
- Hernquist, L. 1989, *Natur*, 340, 687
- Hernquist, L., & Mihos, J. C. 1995, *ApJ*, 448, 41
- Hopkins, P. F., Cox, T. J., Kereš, D., & Hernquist, L. 2008a, *ApJS*, 175, 390
- Hopkins, P. F., Hernquist, L., Cox, T. J., & Kereš, D. 2008b, *ApJS*, 175, 356
- Hopkins, P. F., & Quataert, E. 2010, *MNRAS*, 407, 1529
- Hopkins, P. F., & Quataert, E. 2011, *MNRAS*, 415, 1027
- Hopkins, P. F., Somerville, R. S., Hernquist, L., et al. 2006, *ApJ*, 652, 864
- Hughes, S. A., & Blandford, R. D. 2003, *ApJL*, 585, L101
- Kartalpe, J. S., Dickinson, M., Alexander, D. M., et al. 2012, *ApJ*, 757, 23
- Kellermann, K. I., Sramek, R., Schmidt, M., Shaffer, D. B., & Green, R. 1989, *AJ*, 98, 1195
- Koekemoer, A. M., Faber, S. M., Ferguson, H. C., et al. 2011, *ApJS*, 197, 36
- Laing, R. A., & Peacock, J. A. 1980, *MNRAS*, 190, 903
- Laor, A. 2000, *ApJL*, 543, L111
- Lehmer, B. D., Brandt, W. N., Alexander, D. M., et al. 2005, *ApJS*, 161, 21
- Li, Y., Hernquist, L., Robertson, B., et al. 2007, *ApJ*, 665, 187
- Li, Y.-R., Wang, J.-M., Yuan, Y.-F., Hu, C., & Zhang, S. 2010, *ApJ*, 710, 878
- Lotz, J. M., Jonsson, P., Cox, T. J., et al. 2011, *ApJ*, 742, 103
- Madrid, J. P., Chiaberge, M., Floyd, D., et al. 2006, *ApJS*, 164, 307
- Martel, A. R., Baum, S. A., Sparks, W. B., et al. 1999, *ApJS*, 122, 81
- Martel, A. R., Ford, H. C., Tran, H. D., et al. 2003, *AJ*, 125, 2964
- McKinney, J. C., & Gammie, C. F. 2004, *ApJ*, 611, 977
- McKinney, J. C., Tchekhovskoy, A., & Blandford, R. D. 2012, *MNRAS*, 423, 3083
- McLure, R. J., Willott, C. J., Jarvis, M. J., et al. 2004, *MNRAS*, 351, 347
- Menci, N., Gatti, M., Fiore, F., & Lamastra, A. 2014, *A&A*, 569, A37
- Merritt, D. 2006, *ApJ*, 648, 976
- Narayan, R., & McClintock, J. E. 2012, *MNRAS*, 419, L69
- Podigachoski, P., Barthel, P. D., Haas, M., et al. 2015, *A&A*, 575, 80
- Pudritz, R. E., & Norman, C. A. 1986, *ApJ*, 301, 571
- R Core Team 2014, *R: A Language and Environment for Statistical Computing*, R Foundation for Statistical Computing, Vienna, Austria <http://www.R-project.org>
- Ramos Almeida, C., Bessiere, P. S., Tadhunter, C. N., et al. 2013, *MNRAS*, 436, 997
- Ramos Almeida, C., Bessiere, P. S., Tadhunter, C. N., et al. 2012, *MNRAS*, 419, 687
- Rees, M. J. 1984, *ARA&A*, 22, 471
- Rodriguez-Gomez, V., Genel, S., Vogelsberger, M., et al. 2015, *MNRAS*, 449, 49
- Russell, D. M., Gallo, E., & Fender, R. P. 2013, *MNRAS*, 431, 405
- Sabater, J., Best, P. N., & Heckman, T. M. 2015, *MNRAS*, 447, 110
- Salvati, M., Risaliti, G., Véron, P., & Woltjer, L. 2008, *A&A*, 478, 121
- Sanders, D. B., & Mirabel, I. F. 1996, *ARA&A*, 34, 749
- Sądowski, A., Narayan, R., Tchekhovskoy, A., et al. 2015, *MNRAS*, 447, 49
- Schawinski, K., Simmons, B. D., Urry, C. M., Treister, E., & Glikman, E. 2012, *MNRAS*, 425, L61

- Schnittman, J. D. 2013, *CQGra*, 30, 244007
- Seymour, N., Stern, D., de Breuck, C., et al. 2007, *ApJS*, 171, 353
- Shen, Y., Strauss, M. A., Ross, N. P., et al. 2009, *ApJ*, 697, 1656
- Sikora, M., Stawarz, Ł., & Lasota, J.-P. 2007, *ApJ*, 658, 815
- Simpson, C., Rawlings, S., Ivison, R., et al. 2012, *MNRAS*, 421, 3060
- Skelton, R. E., Whitaker, K. E., Momcheva, I. G., et al. 2014, *ApJS*, 214, 24
- Smith, E. P., & Heckman, T. M. 1989, *ApJ*, 341, 658
- Soltan, A. 1982, *MNRAS*, 200, 115
- Somerville, R. S., Hopkins, P. F., Cox, T. J., Robertson, B. E., & Hernquist, L. 2008, *MNRAS*, 391, 481
- Spinrad, H., Marr, J., Aguilar, L., & Djorgovski, S. 1985, *PASP*, 97, 932
- Steinbring, E. 2011, *AJ*, 142, 172
- Szokoly, G. P., Bergeron, J., Hasinger, G., et al. 2004, *ApJS*, 155, 271
- Tadhunter, C., Dicken, D., Morganti, R., et al. 2014, *MNRAS*, 445, L51
- Tchekhovskoy, A., Narayan, R., & McKinney, J. C. 2011, *MNRAS*, 418, L79
- Terashima, Y., & Wilson, A. S. 2003, *ApJ*, 583, 145
- Treister, E., Schawinski, K., Urry, C. M., & Simmons, B. D. 2012, *ApJL*, 758, L39
- Tundo, E., Tozzi, P., & Chiaberge, M. 2012, *MNRAS*, 420, 187
- Ueda, Y., Watson, M. G., Stewart, I. M., et al. 2008, *ApJS*, 179, 124
- Urrutia, T., Lacy, M., & Becker, R. H. 2008, *ApJ*, 674, 80
- Veilleux, S., Kim, D.-C., & Sanders, D. B. 2002, *ApJS*, 143, 315
- Villforth, C., Hamann, F., Rosario, D. J., et al. 2014, *MNRAS*, 439, 3342
- Volonteri, M., Sikora, M., Lasota, J.-P., & Merloni, A. 2013, *ApJ*, 775, 94
- Wilkes, B. J., Kuraszkiewicz, J., Haas, M., et al. 2013, *ApJ*, 773, 15
- Wilson, A. S., & Colbert, E. J. M. 1995, *ApJ*, 438, 62
- Xu, C., Livio, M., & Baum, S. 1999, *AJ*, 118, 1169
- Xue, Y. Q., Luo, B., Brandt, W. N., et al. 2011, *ApJS*, 195, 10